京都大学防災研究所年報 第 64 号 B
DPRI Annuals, No. 64 B, 2021

Analysis of Future Changes of Geometric Range of Snake Lines and its Relation to Sediment Disasters in a Changing Climate

Ying-Hsin WU, Eiichi NAKAKITA and Akihiko YAMAJI

Synopsis

This study aims to investigate the future changes of sediment disasters with a focus on investigating the patterns of snake line in a changing climate. Constituted by two parameters of hourly rainfall intensity and soil-water index, a snake line is a curve used for early-warning on rainfall-triggered sediment disasters. For reasonably projecting future climate, we adopted high-resolution future climate projections of 2-km and 5-km Non-Hydrostatic Regional Climate Models under the scenarios of RCP2.6 and RCP8.5. Snake lines obtained by climate projections were verified by the reanalyzed precipitation of Radar-AMeDAS. To quantify snake line pattern, we focused on analyzing the geometric range of snake line in terms of the maximal hourly rainfall and soil-water index. Obvious increasing trends for the two parameters and corresponding distributions are revealed on each mesh. Based on six stretching types of snake lines, we examined the spatial distributions and statistics of the future change of snake line patterns under the two scenarios as well as their relation to rainfall prone to sediment disasters. Based on the critical lines, we also demonstrate some statistical features of future hazardous rainfall.

Keywords: climate change, sediment disasters, snake line pattern, NHRCM, Radar-AMeDAS

1. Introduction

In this study, we attempt to quantitatively examine the conditions of sediment disaster in a changing climate. Extreme climate becomes more frequent worldwide to trigger considerable severe water-related disasters, and has raised huge attention of governmental sectors (MLIT, 2020) and scientific communities (Kawamiya et al. 2020; Mori et al., 2021). Recent extreme rainfall events show some obvious changes that rainfall was elongated in the period and intensified in a much higher accumulated amount and peak intensity that have broken new observation records in many places, and, consequently, have triggered numerous devastating floods, landslides and sediment disasters beyond our past experience. Among relevant reasons of extreme weather, one influential factor could be attributed to climate change accompanying increased average earth-surface temperature due to the great amount of greenhouse gas emissions from human activities, which is often termed as global warming phenomenon (Kawamiya et al., 2020 and references therein). As global warming is a long-term heating of the earth's atmosphere, extreme weather would take place more often in the future. Future extreme weather could be altered to possibly amplify occurrence of landslides and sediment hazards in the future.

To practice successful early-warning on landslides and sediment disasters, Ministry of Land, Infrastructure, Transport and Tourism (abbreviated as MLIT) is currently applying the critical line method which utilizes two parameters of hourly rainfall (HR hereafter) and soil-water index (SWI) (Osanai et al., 2010). To constitute a parametric curve of snake lines, the two indices can reflect the influences of short-term peak rainfall and the long-term condition of soil wetness, and could be applied to efficiently assess the

potential occurrence of sediment disasters. Our previous research has explored the future change of disastrous rainfall prone to sediment disasters (Wu et al., 2020). However, until now future characteristics of snake lines in a changing climate has not been examined yet. So, the current study attempts to investigate future snake line patterns with a particular focus on the maximal geometric range of snake lines obtained by high-resolution climate projections. To this end, we adopted the famous 2-km and 5-km Non-Hydrostatic Regional Climate Models (NHRCM, hereafter RCM2 and RCM5, respectively), published by Japan Meteorological Agency (JMA). Also, the 1-km reanalyzed precipitation was used to verify the applicability of snake lines obtained from climate projections. On each mesh, by examining the maximal HR and SWI, we elaborate the future changes of stretching types of snake line patterns as well as the explicit relation to rainfall prone to sediment disasters. Finally, we briefly summarize some statistical features of the hazardous rainfall events in terms of the monthly frequency as well as prefectural future changes. On the other hands, as the hydrometeorological parameters of interest are used for early-warning, the current research could be regarded as a quantitative reference to understand the future status of early-warning alerts for benefiting future disaster management as well as making corresponding policies.

2. Data and method

2.1 JMA Radar-AMeDAS

To confirm applicability of snake lines obtained by climate simulation datasets, we utilized the high-resolution precipitation reanalyzed using observations of 20 C-band radars and the Automated Meteorological Data Acquisition System (AMeDAS) operating by JMA. The dataset is often called Radar-AMeDAS precipitation, and published by JMA routinely. Here we only used the datasets in the period of 2006 to 2020 (15 years in total). The resolutions are 30 minutes in time and 1 km in space. A major benefit holds that the mesh system is exactly the one for all critical lines. For brevity, in what follows Radar-AMeDAS precipitation dataset is abbreviated as JMARA.

2.2 Future projections: 2-km and 5-km NHRCM

The spatiotemporal resolutions are 5 km in space and 30 minutes in time for RCM5, and 2 km in space and 1 hour in time for RCM2. To cover the Japanese archipelago, there are 527×804 grids in RCM5, and 525×1721 grids in RCM2 in a narrower simulation domain. Both have the same ensemble members, as are listed in Table 1. SPA stands for present climate, and the others (SFA_26, SFA_c1, SFA_c2, SFA_c3, and SFA_c0) for future climate. The domain boundary conditions are derived from the simulations of MRI-AGCM3.2S. The scenarios of future projections are set according to Representative Concentration Pathway (RCP) 2.6 and 8.5, proposed in IPCC Fifth Assessment Report in 2014 for representing human activities of industrial development. Four spatial patterns of sea-surface temperature (SST) are imposed as the sea surface boundary conditions in the future projections of RCP8.5. The simulation period of each dataset is 20 years with a one-year time slice and a spin-up period from July 21 to September 1.

To focus on analyzing rainfall-triggered sediment hazards, we directly extracted the parameter of surface

Table 1 Brief information of all NHRCM members (Both for RCM5 and RCM2)

Dataset	Scenario	Boundary SST	Simulation Period
SPA	-	Monthly observation (1979-2003)	from 1980/09/01 to 2000/08/30
SFA_26	RCP2.6	El Niño	from 2076/09/01 to 2095/08/30
SFA_c1	RCP8.5	Less warmer in East tropical Pacific	
SFA_c2	RCP8.5	Stronger El Niño	
SFA_c3	RCP8.5	Warmer in Northwest Pacific	
SFA_c0	RCP8.5	El Niño	

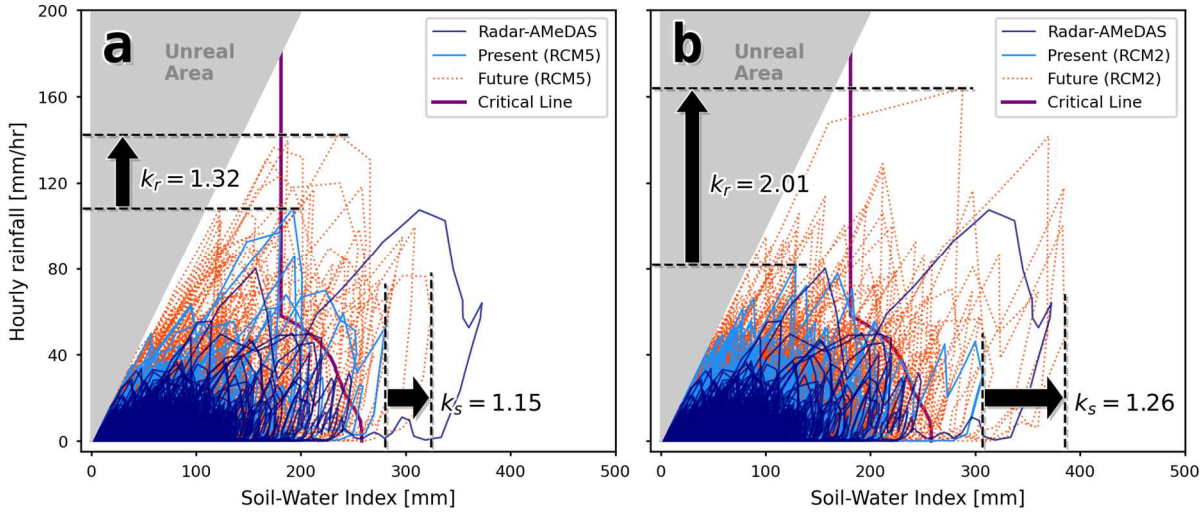

Fig. 1 An illustrative example of comparison among snake lines obtained by a) RCM5, b) RCM2, and Radar-AMeDAS on the mesh of No. 50300668 in Asakura City, Fukuoka prefecture where occurred flooding and massive shallow landslides during 2017 Northern Kyushu heavy rainfall. The definitions of k_r and k_s refer to Equation (1).

precipitation of liquid water (i.e., the parameters of SMQR and RQ1 in RCM5 and RCM2, respectively) without any interpolation. Some relating details of NHRCM can refer to our previous research[4]. Hereafter, for the RCP8.5 scenario, we shall focus on discussing the average property of the four ensemble members without further indication.

2.3 Extraction of parameters and rainfall events

In this study, the 1-km mesh coordinate system of JMARA and for all critical lines is used for analyzing NHRCMs. We processed 15-year JMARA dataset continuously from 2006 to 2020, and processed all datasets of RCM2 and RCM2 following the one-year time slice in the whole dataset period of 20 years. All the processing steps are briefly mentioned as follows. The first is to extract the continuous time series of hourly rainfall on each mesh in each year slice, and then to derive 10-minute rainfall by uniformly extracting original data of one hour or 30 minutes. The extracted 10-minute rainfall series was then used for calculating the continuous time series of SWI by using the conventional method proposed by JMA. To prevent from duplicate counting of a single event, we identified all effective rainfall events (MLIT, 2005; Osanai et al., 2010) with a minimal threshold of 0.5 mm per one hour. Finally, we extracted the maximal HR and SWI in the whole dataset period for examining changes of the geometric range of all snake lines on each mesh. Fig. 1 shows an example on the mesh of 50300668 where is located at E130.85 and N33.39 in Asakura City, Fukuoka prefecture (Takemi 2018; Shakti et al. 2018). The geometric similarity of the snake lines from RCM5 and RCM2 are confirmed with the ones from JMARA. Obviously, we can observe the extension of the range of snake lines from both NHRCMs. Therefore, in what follows we shall try to systematically quantify the characteristics of these geometric changes and their relation to hazardous rainfall prone to sediment disasters.

Besides, from all datasets of NHRCMs, the time series of HR and SWI were checked to judge whether any pairs of the two parameters on each mesh pass through the corresponding critical line of that mesh. On each mesh, within one effective rainfall event, we only counted one hazardous rainfall event no matter how many times the critical line was crossed. The event herein is not related to the one of any storm or rainfall system from the viewpoint of meteorology.

3. Results and discussion

3.1 Comparison with Radar-AMeDAS

To confirm the applicability of snake lines obtained from NHRCMs, we compared them with the ones from JMARA. Although the evolution of snake line could

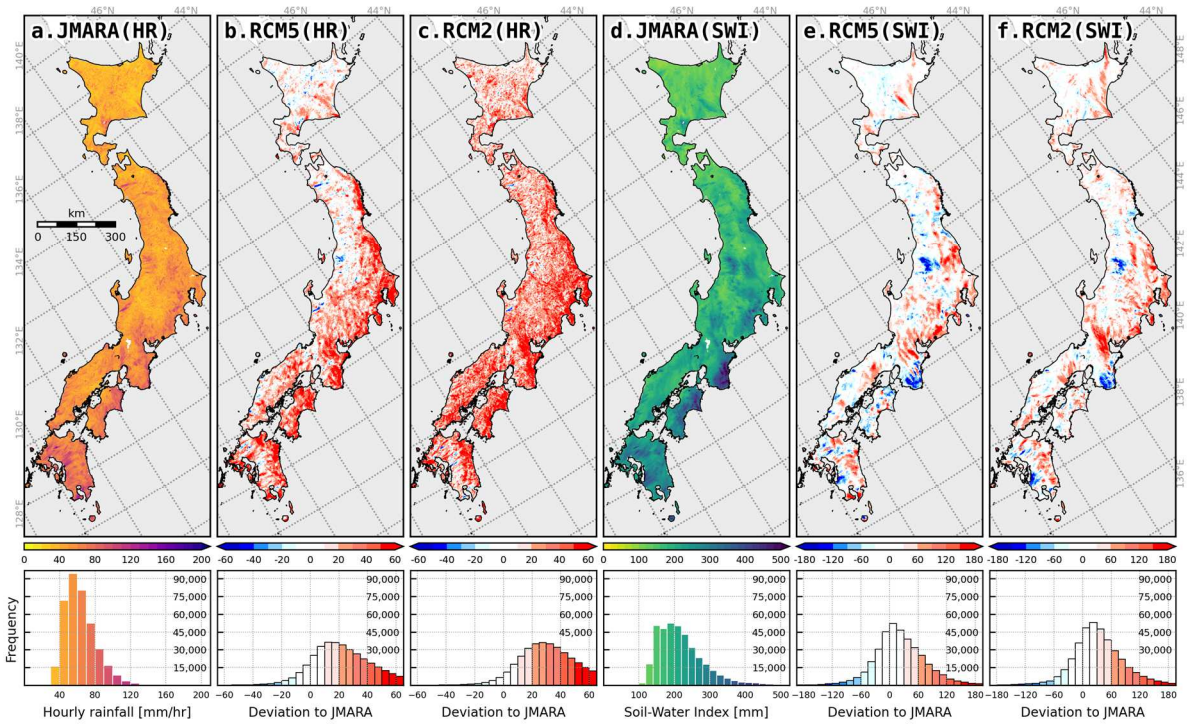

Fig. 2 Comparison of the maximal hourly rainfall (HR) in a)-c) and soil-water index (SWI) in d)-f) among Radar-AMeDAS and the present climate datasets of RCM5 and RCM2. The deviations are shown in b) and c) for the maximal HR to Radar-AMeDAS, and e) and f) for the maximal SWI, respectively. Lower row shows the corresponding histograms.

reflect some important features of sediment disaster occurrence, we only focus on the maximal values of HR and SWI to reveal the geometric range of a snake lines in the current analysis. Fig. 2 shows the deviations of the maximal HR and SWI among JMARA and the present climate datasets of RCM5 and RCM2. Obviously, as are shown in Fig. 2b and Fig. 2c, the maximal HR from NHRCMs is much higher than JMARA in almost all places, particularly in the Pacific Ocean side. There are 82.2% of meshes with positive deviation in RCM5 and 92.5% in RCM2. On the other hand, in Fig. 2e and Fig. 2f, the maximal SWI does not deviate much in RCM5, but slightly in the positive direction in RCM2. Sharp rise can be seen in Mie, Aichi, east Kyushu, and Tokai regions. Then, obvious declines can be found in Wakayama, east Kumamoto, and Bandai-Asahi National Park from both NHRCMs.

So far, it has shown the deviations of the maximal HR and SWI in the present climate datasets of NHRCMs to JMARA. However, it is still unclear to straightforwardly understand features of the future changes of the two parameters merely with respect to their deviations to the present climate dataset. In what follows, we turn to use relative ratios to explain future changes of the two hydrometeorological parameters of HR and SWI.

3.2 Future changes of maximal hourly rainfall and Soil-Water Index

Before analyzing snake line patterns, we aim to separately investigate future changes of the maximal HR and SWI, as are illustrated in Fig. 3 and Fig. 4, respectively. To express changes, the scale factors of HR and SWI on each mesh are respectively given as

$$k_r = \frac{HR_{\mathrm{SFA}}}{HR_{\mathrm{SPA}}} \quad \text{and} \quad k_s = \frac{SWI_{\mathrm{SFA}}}{SWI_{\mathrm{SPA}}}, \tag{1}$$

where the subscripts of SPA and SFA denote the present and future climate datasets, and HR and SWI hereafter denote the maximal values in the whole dataset periods. Based on the definition of Eq. (1), there would be no significant change if the scale factor $k \to 1$, and there are 50% of decline or 2 times of

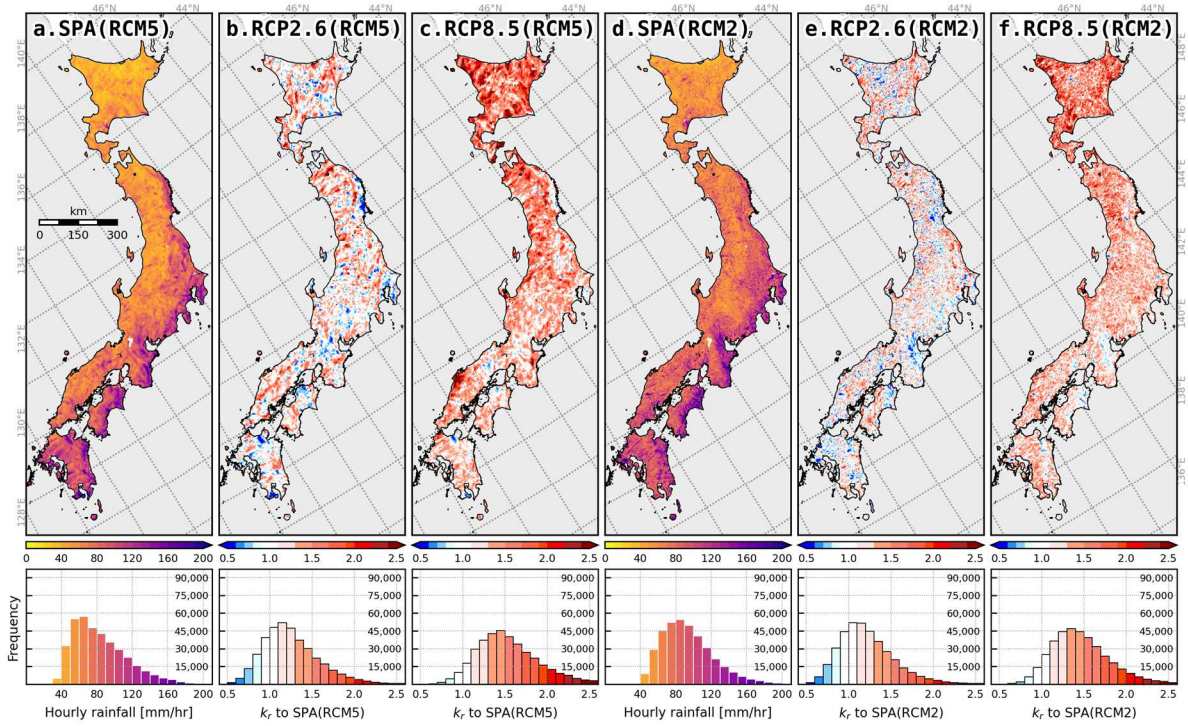

Fig. 3 Future changes of the maximal HR from RCM5 in a)-c) and RCM2 in d)-f). The scale factor k_r denotes the ratio of future projections under different scenarios to present climate (SPA). The lower row shows the corresponding histograms.

increase when $k \to 0.5$ and 2, respectively. To gently remind, a higher value of the two scale factors does not guarantee a higher absolute value of the corresponding parameter.

For the features of HR, Fig. 3 demonstrates that the distributions of the scale factor k_r under the RCP2.6 scenario show no obvious increasing trend along the Japanese archipelago, but the distributions under RCP8.5 present clear rising trends everywhere except some regions in west Japan (e.g., Mie, Aichi, south Hyogo, east Shikoku, and north Kyushu). Significant rises of $k_r \approx 2.0$ appear in Tohoku and Hokkaido regions. The highest frequencies of the factor k_r under RCP2.6 and RCP8.5 reach around 1.1 and 1.3, respectively. In contrast to HR, both in the NHRCMs the scale factor k_s of the maximal SWI shows that 58% of meshes have increasing trends under RCP2.6, and 85% under RCP8.5. Particularly, the distributions of k_s under the same scenario are quite similar between RCM5 and RCM2. Also, as is shown in Fig. 4, obvious decline trends of SWI can be found in Mie, Aichi, Hyogo, and Fukuoka prefectures under RCP2.6. For this results, it could be considered that the decline of SWI might represent the condition that soil may be dryer, but further investigation is required to verify this possible condition of soil wetness which is one of essential influential factors for occurrence of landslides and sediment hazards.

To sum up, we have quantified the future changes of the maximal HR and SWI separately. It can be found an obvious increasing future trends of the maximal HR, but just a mild one of the maximal SWI. Then, we shall examine features of the combination of the two parameters.

3.3 Future changes of snake line patterns

To express geometric changes of the range of snake lines on the phase plane by the scale factors k_r and k_s, the six types of stretching of snake line are defined as below

$$\left.\begin{array}{lll} \text{Type-A:} & k_r > 1.5, & k_s > 1.5 \\ \text{Type-B:} & 1.05 < k_r \le 1.5, & 1.05 < k_s \le 1.5 \\ \text{Type-C:} & k_r > 1.05, & k_s \le 0.95 \\ \text{Type-D:} & k_r \le 0.95, & k_s > 1.05 \\ \text{Type-E:} & 0.95 < k_r \le 1.05, & 0.95 < k_s \le 1.05, \\ \text{Type-F:} & k_r \le 0.95, & k_s \le 0.95, \end{array}\right\} \quad (2)$$

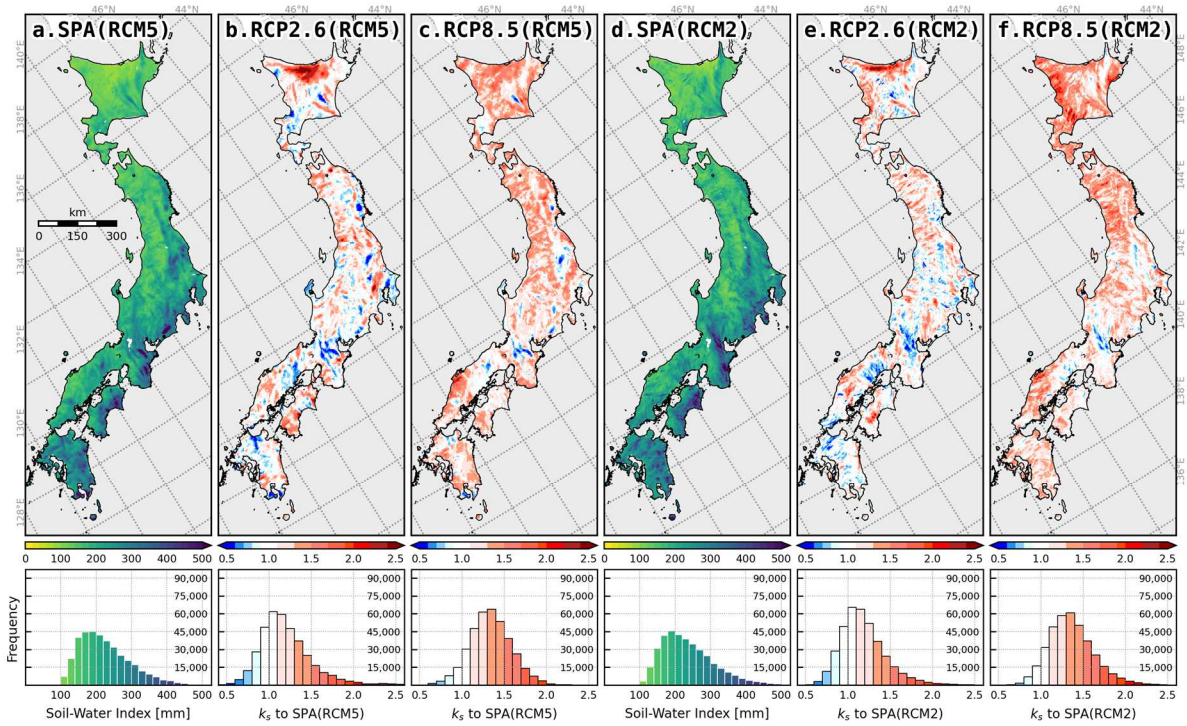

Fig. 4 Future changes of the maximal SWI from RCM5 in a)-c) and RCM2 in d)-f) in terms of the scale factor k_s. The scale factor k_s denotes the ratio of future projections under different scenarios to present climate (SPA). The lower row shows the corresponding histograms.

with a given tolerance range of $\pm 5\%$ at unity. In the practical sense, the stretching of Type-A and Type-B represent that rainfall is intensified in the amount and extended in a longer duration; Type-C may reflect that rainfall is intensified in a shorter duration; Type-D stands for a duration-prolonged rainfall in a higher accumulated amount but with a lower peak intensity. This rainfall type could be prone to deep-seated landslides. Type-E represents no significant changes. Finally, Type-F stands for rainfall weakened both in intensity and duration. All these types are used for simply categorizing future changes of the geometric range of snake lines, or says snake line patterns.

Fig. 5 demonstrates the distributions and histograms of the six stretch types. Both in the NHRCMs, 30% of meshes are categorized as the Type-A and Type-B representing obvious enlargement of snake lines under RCP2.6, and 70% under RCP8.5. Also, the Type-A meshes (about 10%) are mostly distributed in Shimane prefecture, Tohoku and Hokkaido regions under RCP8.5. For all of the conditions of enlargement of snake lines (Type-A, Type-B, Type-C, and Type-D), from both of RCM5 and RCM2 there are around 80% and 60% of meshes under RCP8.5 and RCP2.6, respectively. The Type-C and Type-D, representing partial enlargement of snake lines, would be declined more in the scenario of RCP8.5 than the one of RCP2.6. Particularly, for the Type-D which may be prone to deep-seated landslides, it can be found 4.9 and 2.6% of meshes under the scenario of RCP8.5 from RCM5 and RCM2, respectively, and 11.8 and 9.6% under RCP2.6. Then, under RCP2.6 and RCP8.5 there are respectively around 28% and 16% of meshes having insufficient changes of snake line range. Finally, under both scenarios the distributions of the meshes in Type-F that both scale factors shrink are mainly in agreement with the places with $k_s < 0.95$ in Fig. 4. Another particular point is that, both in the RCM5 and RCM2, the distributions and histograms under the same scenario coincide well with each other.

The future changes of the geometric range of snake line on each mesh have been quantitatively derived. In our limited understanding, as an additional advantage of the present analysis, it is believed that all these features could help suggest the location of meshes for

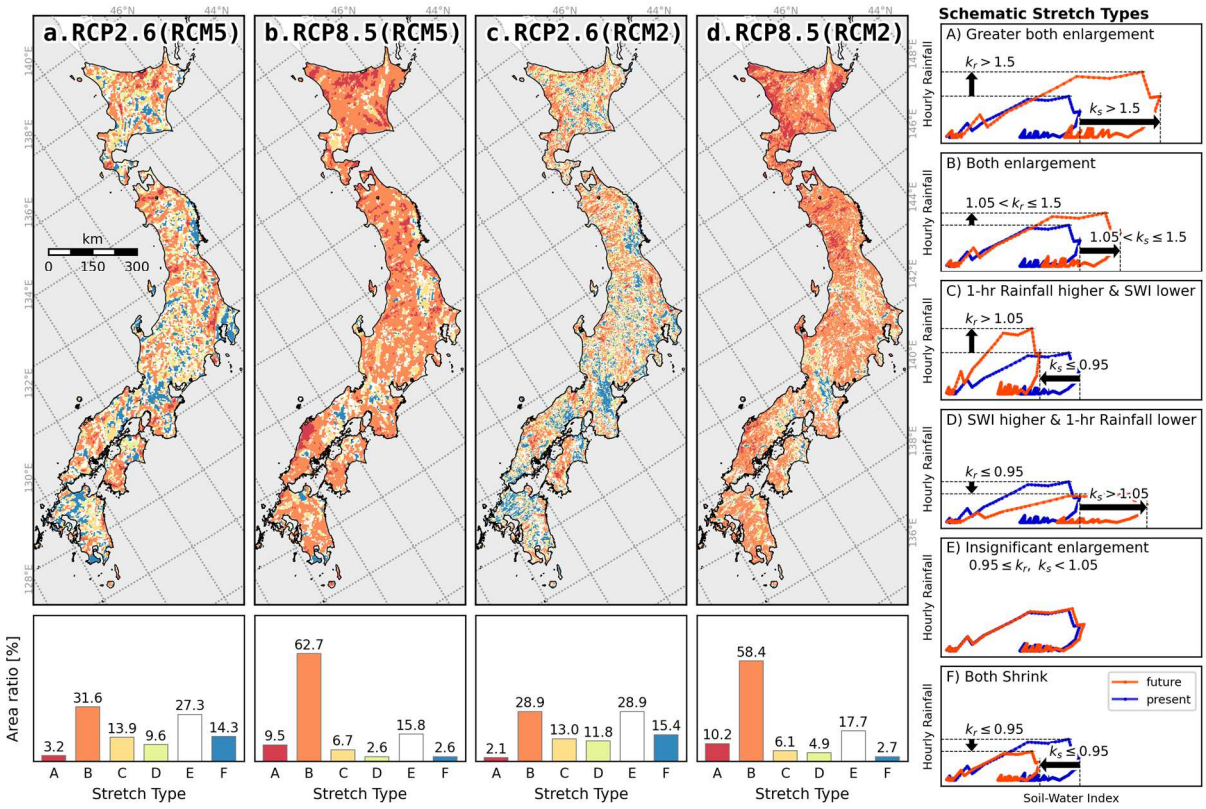

Fig. 5 Future changes of snake line patterns categorized by six stretch types in terms of the maximal HR and SWI. Schematic examples of the six stretch types are shown on the right. Subfigures a) and b) show the results of RCM5; c) and d) the results of RCM2. The lower row on the left presents the ratios of the total number of the meshes of each stretch type to the total mesh number.

the re-examination or adjustment of the corresponding critical lines for better efficiency of early-warning.

3.4 Hazardous rainfall distribution

To find the relation between the stretching of snake line with hazardous rainfall, the critical line on each mesh was applied to the calculated time series of HR and SWI for counting rainfall events prone to sediment disasters. Fig. 6 demonstrates the results of spatial distributions and the corresponding histograms in terms of monthly frequency. To gently remind, the hazardous rainfall event is counted with respect to the mesh-based critical line method, not to any storm or rainfall system. By courtesy of MLIT and all prefectural governments, all of the critical lines being applying for the current early-warning practice are obtained for our analysis. Despite the discrepancy of the spatial resolutions of NRCHMs, the distributions of hazardous rainfall events are in good agreement with each other, but the histograms present slight difference in monthly frequency. These histograms clearly show that the occurrence of hazardous rainfall events concentrates on the wet season from May to October, and is much intensified in the summer from July to September under RCP8.5. It can be observed a particular condition that, under the scenario of RCP8.5 in both NHRCMs, the error bars show low deviations of extracted hazardous rainfall events in July, but much higher ones in August and September that would suggest further investigations to identify physical conditions of dominant rainfall as well as the relating ambient atmospheric status.

Although only analyzing the precipitation of liquid water, we can still observe very few hazardous rainfall events in the winter season. In each dataset, the total counts from December to next year's March are all less than 1.0% of total counts. Moreover, comparison between Fig. 5 and Fig. 6 reveals one particular condition that the places with decreasing trends of hazardous rainfall events just satisfactorily match with

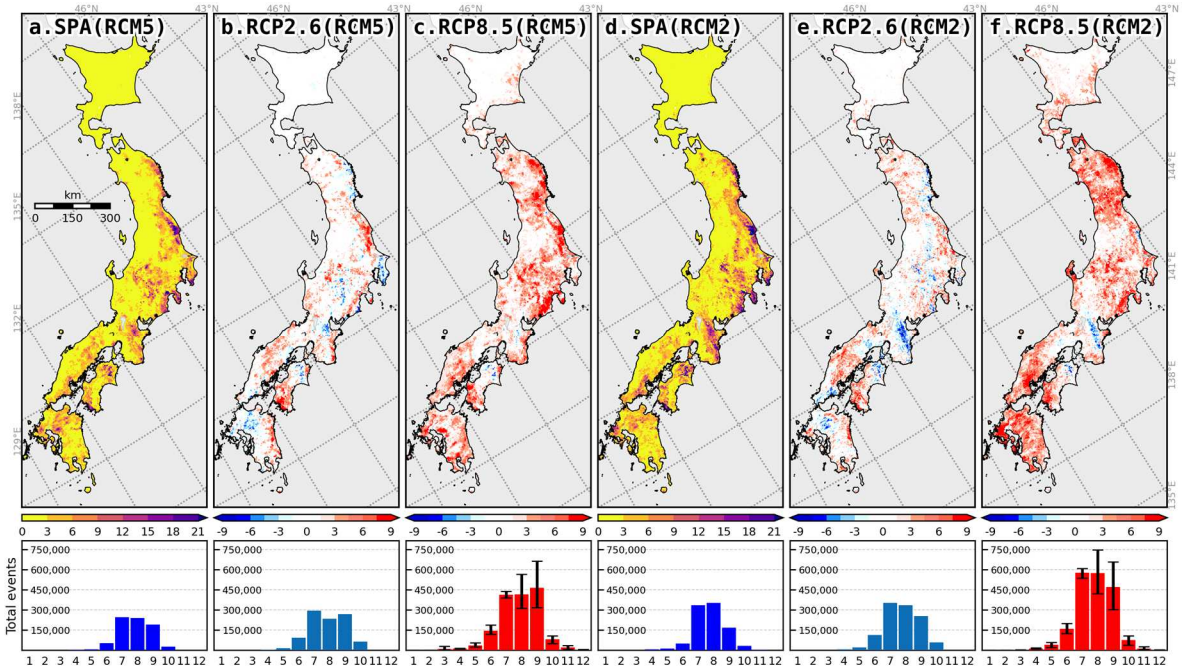

Fig. 6 The count and deviation of hazardous rainfall prone to sediment disasters from RCM5 and RCM2: a) and d) show the total events in the present climate (SPA). b) and e) are the deviations of the RCP2.6 result to SPA of each model. c) and f) show the deviations of RCP8.5. The lower row demonstrates the corresponding total counts of hazardous rainfall event, and the error bars in c) and f) denote the maximum and minimum. The total counts in RCM2 is around 21% more than RCM5.

the meshes in the stretch Type-F. But, the count of hazardous rainfall event would not definitely be elevated at the meshes which are categorized as the stretch Type-A and Type-B, representing enlargement in both directions on the phase plane of snake line. So far, it has been shown the spatial distribution of hazardous rainfall.

As we noticed the deviations from the histograms in Fig. 6, we further examine the temporal features in terms of monthly frequency. To link with the spatial distribution, Fig. 7 shows the monthly frequency normalized by the mesh number of each geographical region of Japan. The particular findings are that the extracted hazardous rainfall are concentrated in July in the regions of Japanese Sea Side, but uniformly distributed in the summer season from July to September with a slight elevated normalized frequency in September in the regions of Pacific Ocean Side. In Okinawa, it can be seen that the extracted events are distributed all year long except the winter season. On the other hand, we can also observe the obvious increase of extracted events from the scenario of RCP8.5 out of the one of RCP2.6. Compilation of the results from both high-resolution NHRCMs could provide more reliable assessment than the one in our previous research (Wu et al., 2020).

4. Conclusions

This study investigates the future snake line patterns and their relation to sediment disasters in a changing climate by considering the geometric range on the phase plane of snake line constituted by the maximal hourly rainfall and soil-water index. With the application of the most current high-resolution future protections, the present analysis results reveal that the future change of the maximal hourly rainfall is enlarged much higher than the maximal soil-water index. Also, the soil-water index would decline in accompany with the declination of the count of hazardous rainfall prone to sediment disasters. As this study only examined the maximal geometric range of snake lines, it is still open to answer temporal features of snake line evolution in a changing climate.

Last, and the most importantly, it is believed that this study could practically benefit understanding of

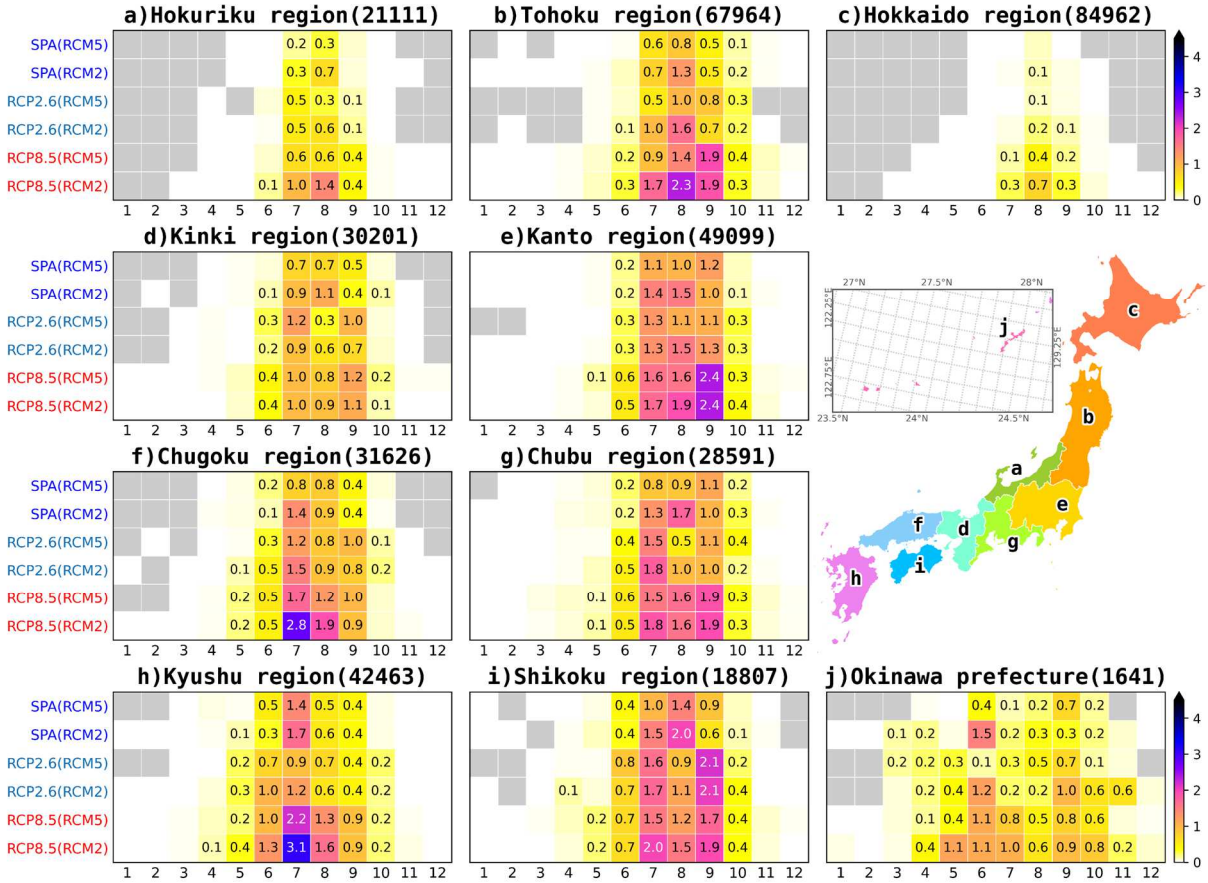

Fig. 7 The monthly frequency of hazardous rainfall normalized by the total number of 1-km mesh of graphical regional: a) Hokuriku, b) Tohoku, c) Hokkaido, d) Kinki, e) Kanto, f) Chugoku, g) Chubu, h) Kyushu, i) Shikoku regions, and j) Okinawa prefecture from RCM5 and RCM2. The numbers in the brackets denote the total number of mesh in each region.

conditions of early-warning on rainfall-triggered landslides and sediment disasters in a changing climate.

Acknowledgments

This work was supported by the Integrated Research Program for Advancing Climate Models (TOUGOU) Grant Number JPMX-D0717935498 from the Ministry of Education, Culture, Sports, Science and Technology (MEXT), Japan. The authors appreciate the valuable data of all the latest critical lines from MLIT Sabo Planning Division, JMA, and all prefectural governments.

References

Kawamiya, M., Ishii, M., Mori, N., Nakakita, E., Takayabu, I. and Watanabe, M. (2021): Preface for "Projection and impact assessment of global change," Prog. Earth Planet. Sci., Vol. 8, 30.

MLIT (2005): Manual of Determining Rainfall Threshold for Early-Warning of Sediment Disasters.

MLIT (2020): Committee Discussions on Technology and Evaluation of Sediment Disasters under Climate Change.

Mori, N., Takemi, T., Tachikawa, Y., Tatano, H., Shimura, T., Tanaka, T., Fujimi, T., Osakada, Y., Webb, A. and Nakakita, E. (2021): Recent nationwide climate change impact assessments of natural hazards in Japan and East Asia. Weather Clim. Extrem., Vol. 32, 100309.

Osanai, N., et al. (2010): Japanese early-warning for debris flows and slope failures using rainfall indices with Radial Basis Function Network, Landslides, Vol. 7, pp. 325-338.

Shakti, P.C., Nakatani, T. and Misumi, R. (2018):

Hydrological Simulation of Small River Basins in Northern Kyushu, Japan, During the Extreme Rainfall Event of July 5–6, 2017. J. Disaster Res., Vol. 13, No. 2, pp. 396-409.

Takemi, T. (2018): Importance of Terrain Representation in Simulating a Stationary Convective System for the July 2017 Northern Kyushu Heavy Rainfall Case. SOLA, Vol. 14, pp. 153-158.

Wu, Y.-H., Nakakita, E. and Kunitomo, M. (2020): Future change of rainfall-triggered landslide risk using NHRCM05 based on critical line method, Jour. Japan Society of Civil Engineers, Ser. B1 (Hydraulic Eng.), Vol. 76, No. 2, pp. I_67-I_72.

(Received August 31, 2021)